

Time-dependent optimized coupled-cluster method for multielectron dynamics III: A second-order many-body perturbation approximation

Himadri Pathak,^{1, a)} Takeshi Sato,^{1, 2, 3, b)} and Kenichi L. Ishikawa^{1, 2, 3, c)}

¹⁾Department of Nuclear Engineering and Management, School of Engineering, The University of Tokyo, 7-3-1 Hongo, Bunkyo-ku, Tokyo 113-8656, Japan

²⁾Photon Science Center, School of Engineering, The University of Tokyo, 7-3-1 Hongo, Bunkyo-ku, Tokyo 113-8656, Japan

³⁾Research Institute for Photon Science and Laser Technology, The University of Tokyo, 7-3-1 Hongo, Bunkyo-ku, Tokyo 113-0033, Japan

(Dated: 5 June 2020)

We report successful implementation of the time-dependent second-order many-body perturbation theory using optimized orthonormal orbital functions called time-dependent optimized second-order many-body perturbation theory [TD-OMP2] to reach out to relatively larger chemical systems for the study of intense-laser-driven multielectron dynamics. We apply this method to strong-field ionization and high-order harmonic generation (HHG) of Ar. The calculation results are benchmarked against *ab initio* time-dependent complete-active-space self-consistent field (TD-CASSCF), time-dependent optimized coupled-cluster double (TD-OCCD), and time-dependent Hartree-Fock (TDHF) methods, as well as a single active electron (SAE) model to explore the role of electron correlation.

I. INTRODUCTION

Laser-driven multielectron dynamics has become an active area of research, thanks to the remarkable advance in laser technologies, which has made it possible to measure and control the electronic motion^{1–10}. Atoms and molecules interacting with laser pulses of intensity $\gtrsim 10^{14}$ W/cm² in the visible to mid-infrared spectral range, exhibit highly, even nonperturbatively nonlinear response such as above-threshold ionization (ATI), tunneling ionization, nonsequential double ionization (NSDI), and high-order harmonic generation (HHG). The HHG process is one of the key elements in the study of light-matter interaction in the attosecond time-scale, delivering ultrashort coherent light pulses in the extreme-ultraviolet (XUV) to the soft x-ray regions, which carry the information on the electronic structure and dynamics of the generating medium.¹¹ The HHG spectra are characterized by a plateau where the intensity of the emitted radiation remains nearly constant up to many orders, followed by an abrupt cutoff.

In principle, the multielectron dynamics and electron correlation^{12–15} are exactly described by the time-dependent Schrödinger equation (TDSE). However, direct numerical integration of TDSE is not feasible for systems with more than two electrons^{16–25}. As a result, single-active-electron (SAE) approximations has been widely used^{26,27}, in which only the outermost electron is explicitly treated under the effect of the other electrons modeled by an effective potential. Whereas SAE has been useful in numerically exploring different strong-

field phenomena, the electron correlation is missing in this approximation.

Therefore, various tractable *ab initio* methods have actively been developed for theoretical description of correlated multielectron dynamics in intense laser fields. Among the most reliable approaches to serve the purpose are the multiconfiguration time-dependent Hartree-Fock (MCTDHF) method^{28–32} and time-dependent complete-active-space self-consistent-field (TD-CASSCF) method^{33,34}. In MCTDHF, the electronic wavefunction is expressed in terms of full configuration interaction (FCI) expansion, $\Psi(t) = \sum_{\mathbf{I}} C_{\mathbf{I}}(t)\Phi_{\mathbf{I}}(t)$, where both CI coefficients $\{C_{\mathbf{I}}(t)\}$ and *occupied* spin-orbitals $\{\psi_p(t)\}$ constituting Slater determinants $\{\Phi_{\mathbf{I}}(t)\}$ are propagated in time. The TD-CASSCF method flexibly classifies occupied orbital space into *frozen-core* (doubly occupied and fixed in time), *dynamical-core* (doubly occupied but propagated in time) and *active* (fully correlated and propagated in time) subspaces. Though accurate and powerful, the computational cost of the MCTDHF and TD-CASSCF methods scales factorially with the number of correlated electrons.

More approximate and thus less demanding methods such as the time-dependent restricted-active-space self-consistent field (TD-RASSCF),^{35–37} and time-dependent occupation-restricted multiple-active-space (TD-ORMAS)³⁸ have been developed by further flexibly classifying *active* orbital sub-space to target larger chemical systems by limiting CI expansion of the wavefunction up to a manageable level. The TD-RASSCF and TD-ORMAS methods achieve a polynomial, instead of factorial, cost scaling, and state-of-the-art real-space implementations have turned out to be of great utility.^{34,37,39,40} (See Ref. 12 for a review of *ab initio* wavefunction-based methods for multielectron dynamics, Ref. 41 and references therein for extension to correlated electron-nuclear dynamics, and Ref. 42 for a perspec-

^{a)}Electronic mail: pathak@atto.t.u-tokyo.ac.jp

^{b)}Electronic mail: sato@atto.t.u-tokyo.ac.jp

^{c)}Electronic mail: ishiken@n.t.u-tokyo.ac.jp

tive on multiconfiguration approaches for indistinguishable particles.) Nevertheless, truncated-CI-based methods, even with time-dependent orbitals, have a general drawback of not being size extensive.

To regain the size-extensivity at the same level of truncation, we have recently derived and numerically implemented a time-dependent optimized coupled-cluster (TD-OCC) method⁴³ using optimized orthonormal orbitals where both orbitals and amplitudes are time-dependent. Our TD-OCC method is the time-dependent formulation of the stationary orbital optimized coupled-cluster method.^{44,45} We have implemented the TD-OCC method with up to triple excitation amplitudes (TD-OCCD and TD-OCCDT), and applied it to multielectron dynamics in Ar induced by a strong laser pulse to obtain a good agreement with the fully-correlated TD-CASSCF method within the same active orbital space. In earlier work, Kvaal reported⁴⁶ an orbital adaptive coupled-cluster (OATDCC) method built upon the work of Arponen using biorthogonal orbitals;⁴⁷ though, applications to laser-driven dynamics have not been addressed. The polynomial scaling TD-OCC⁴³ or the OATDCC⁴⁶ method can reduce the computational cost to a large extent in comparison to the general factorially scaling MCTDHF methods.

As a cost-effective approximation of the TD-OCCD method, we have recently developed a method called TD-OCEPA0⁴⁸ based on the simplest version of the coupled-electron pair approximation,^{49–54} or equivalently the linearized CCD approximation,⁵⁵ popular in quantum chemistry. The computational cost of the TD-OCEPA0 method scales as N^6 , with N being the number of active orbitals. Although this is the same scaling as that of the parent TD-OCCD method, TD-OCEPA0 is much more efficient than TD-OCCD due to the linearity of amplitude equations and avoidance of a separate solution for the de-excitation amplitudes, resulting from the Hermitian structure of the underlying Lagrangian.⁴⁸

To enhance the applicability to even larger chemical systems, we are looking for further approximate versions with a lower computational scaling in the TD-OCC framework. The coupled-cluster method is intricately connected with the many-body perturbation theory. It allows one to obtain finite-order perturbation theory energies and wavefunction from the coupled-cluster equations.⁵⁶ The computation of the second-order energy requires the first-order wavefunction, and only doubly excited determinants have contributions in the first-order correction to the reference wavefunction. Thus, second-order many-body perturbation theory (MP2) can be seen as an approximation to the coupled-cluster double (CCD) method, having a lower N^5 scaling.

The MP2 method with optimized orbitals has been developed by Bozkaya *et al.*⁵⁷ for the stationary electronic structure calculations by minimization of the so-called MP2- Λ functional. In earlier work, the optimization of the MP2 energy was based on the minimization of the Hylleraas functional with respect to the orbital

rotation.^{58,59} While both of these techniques provide identical energy at the stationary point, the Λ functional-based derivation has an advantage that it can be easily extended to higher-order many-body perturbation theory.⁶⁰

In this article, we propose time-dependent orbital optimized second-order many-body perturbation theory (TD-OMP2) as an approximation to the TD-OCCD method, based on the time-dependent (quasi) variational principle. The TD-OMP2 method inherits important features of size extensivity and gauge invariance from TD-OCC, with a reduced computational cost of $O(N^5)$. As a first test case, we apply the TD-OMP2 method to electron dynamics in Ar atom irradiated by a strong laser field, and compare the results with those computed at SAE, TDHF, TD-OCCD, and TD-CASSCF levels to understand where really TD-OMP2 stands in describing the effects of correlation in the laser-driven multielectron dynamics. It should be emphasized that the present TD-OMP2 method, albeit named after a perturbation theory, can be applied to laser-induced, nonperturbative electron dynamics, since the laser-electron interaction is fully (nonperturbatively) included in the zeroth-order description with time-dependent orbitals.

This paper is organized as follows. Our formulation of the TD-OMP2 method is presented in Sec. II. Numerical applications are described and discussed in Sec. III. The concluding remarks are given in Sec. IV. Hartree atomic units are used unless otherwise stated, and Einstein convention is implied throughout for summation over orbital indices.

II. TD-OMP2 METHOD

Let us consider the electronic Hamiltonian H of the following form,

$$H = \sum_i^{N_e} h(\mathbf{r}_i, \mathbf{p}_i) + \sum_{i < j}^{N_e} \frac{1}{|\mathbf{r}_i - \mathbf{r}_j|}, \quad (1)$$

$$h(\mathbf{r}, \mathbf{p}) = h_0(\mathbf{r}, \mathbf{p}) + V_{\text{ext}}(\mathbf{r}, \mathbf{p}, t), \quad (2)$$

where N_e is the number of electrons, \mathbf{r}_i and \mathbf{p}_i are the position and canonical momentum, respectively, of electron i , h_0 is the field-free one-electron Hamiltonian, and V_{ext} is the laser-electron interaction. The Hamiltonian in the second-quantization notation can be written as,

$$\hat{H} = \hat{h} + \hat{v}, \quad (3)$$

$$\hat{h} = h_\nu^\mu \hat{E}_\nu^\mu, \quad \hat{v} = \frac{1}{2} u_{\nu\lambda}^{\mu\gamma} \hat{E}_{\nu\lambda}^{\mu\gamma} = \frac{1}{4} v_{\nu\lambda}^{\mu\gamma} \hat{E}_{\nu\lambda}^{\mu\gamma}, \quad (4)$$

where $\hat{E}_\nu^\mu = \hat{c}_\mu^\dagger \hat{c}_\nu$, $\hat{E}_{\nu\lambda}^{\mu\gamma} = \hat{c}_\mu^\dagger \hat{c}_\lambda^\dagger \hat{c}_\lambda \hat{c}_\nu$, and \hat{c}_μ^\dagger (\hat{c}_μ) is the creation (annihilation) operator for the set of orthonormal $2n_{\text{bas}}$ spin-orbitals $\{\psi_\mu\}$, with n_{bas} being the number of basis functions (or grid points) to represent the spatial

TABLE I. Comparison of ground state energy (in Hartree) of BH molecule in DZP basis with PSI4⁶¹ program package.

Bond Length (bohr)	MP2		OMP2	
	this work	PSI4 ⁶¹	this work	PSI4 ⁶¹
1.8	-25.149288192	-25.149288192	-25.149565428	-25.149565428
2.0	-25.183068430	-25.183068429	-25.183367319	-25.183367319
2.2	-25.196855310	-25.196855310	-25.197186611	-25.197186611
2.4(r_e)	-25.198570797	-25.198570797	-25.198947432	-25.198947432
2.8	-25.183573786	-25.183573786	-25.184093435	-25.184093435
3.2	-25.159043339	-25.159043339	-25.159809546	-25.159809546
3.6	-25.133018128	-25.133018128	-25.134185728	-25.134185728
4.0	-25.108605403	-25.108605402	-25.110381925	-25.110381924
5.0	-25.059981388	-25.059981388	-25.064548176	-25.064548176
6.0	-25.029750598	-25.029750598	-25.039814328	-25.039814327
7.0	-25.016553779	-25.016553780	-25.037103689	-25.037103689

Gaussian09 program⁶² is used to generate the required one-electron, two-electron and the overlap integrals, required for the imaginary time propagation of EOMs in the orthonormalized gaussian basis. A convergence cut off of 10^{-15} Hartree of energy difference is chosen in subsequent time steps.

part of ψ_μ . The operator matrix elements h_ν^μ , $u_{\nu\lambda}^{\mu\gamma}$, and $v_{\nu\lambda}^{\mu\gamma}$ are defined as

$$h_\nu^\mu = \int dx_1 \psi_\mu^*(x_1) h(\mathbf{r}_1, \mathbf{p}_1) \psi_\nu(x_1), \quad (5)$$

$$u_{\nu\lambda}^{\mu\gamma} = \int \int dx_1 dx_2 \frac{\psi_\mu^*(x_1) \psi_\gamma^*(x_2) \psi_\nu(x_1) \psi_\lambda(x_2)}{|\mathbf{r}_1 - \mathbf{r}_2|}, \quad (6)$$

and $v_{\nu\lambda}^{\mu\gamma} = u_{\nu\lambda}^{\mu\gamma} - u_{\lambda\nu}^{\mu\gamma}$, where $x_i = (\mathbf{r}_i, \sigma_i)$ is a spatial-spin coordinate. The complete set of $2n_{\text{bas}}$ spin-orbitals (labeled with $\mu, \nu, \gamma, \lambda$) is divided into n_{occ} *occupied* (o, p, q, r, s) and $2n_{\text{bas}} - n_{\text{occ}}$ *virtual* spin-orbitals having nonzero and vanishing occupations, respectively, in the total wavefunction. The occupied spin-orbitals are classified into n_{core} *core* spin-orbitals which are occupied in the reference Φ and kept uncorrelated, and $n_{\text{act}} = n_{\text{occ}} - n_{\text{core}}$ *active* spin-orbitals (t, u, v, w) among which the $N_{\text{act}} = N_e - n_{\text{core}}$ active electrons are correlated. The active spin-orbitals are further split into those in the *hole* space (i, j, k, l) and the *particle* space (a, b, c, d), which are defined as those occupied and unoccupied, respectively, in the reference Φ . The core spin-orbitals can further be split into *frozen-core* space (i'', j'') and the *dynamical-core* space (i', j'). The frozen-core orbitals are fixed in time, whereas dynamical core orbitals are propagated in time.³³ (See Fig. 1 of Ref. 43 for a pictorial illustration of the orbital subspace.)

A. Review of TD-OCCD

The stationary MP2 method can be considered as an approximation of the CCD method, where the full CCD energy functional,

$$E = \langle \Phi | (1 + \hat{\Lambda}_2) e^{-\hat{T}_2} \hat{H} e^{\hat{T}_2} | \Phi \rangle \quad (7)$$

is approximated by retaining the terms giving the second-order correction to the reference energy $E_0 = \langle \Phi | \hat{H} | \Phi \rangle$. Here, $\hat{T}_2 = \tau_{ij}^{ab} \hat{E}_{ij}^{ab}$ and $\hat{\Lambda}_2 = \lambda_{ab}^{ij} \hat{E}_{ab}^{ij}$, with τ_{ij}^{ab} and λ_{ab}^{ij} being the excitation and de-excitation amplitudes, respectively. Therefore, we start with the time-dependent CCD Lagrangian of the following form,

$$L(t) = \langle \Phi | (1 + \hat{\Lambda}_2) e^{-\hat{T}_2} (\hat{H} - i\partial_t) e^{\hat{T}_2} | \Phi \rangle, \quad (8)$$

which is a natural time-dependent extension of the energy functional, Eq. (7). Following Ref. 43, we consider the real-valued action functional,

$$S = \Re \int_{t_0}^{t_1} L(t) dt = \frac{1}{2} \int_{t_0}^{t_1} \{L(t) + L^*(t)\} dt, \quad (9)$$

and make it stationary, $\delta S = 0$, with respect to the variation of amplitudes $\delta\tau_{ij}^{ab}$, $\delta\lambda_{ab}^{ij}$ and variations of orthonormality-conserving orbitals $\delta\psi_\nu$. The equations of motion (EOMs) for the amplitudes are obtained as

$$i\dot{\tau}_{ij}^{ab} = \langle \Phi_{ij}^{ab} | e^{-\hat{T}_2} (\hat{H} - i\hat{X}) e^{\hat{T}_2} | \Phi \rangle, \quad (10)$$

$$-i\dot{\lambda}_{ab}^{ij} = \langle \Phi | (1 + \hat{\Lambda}_2) e^{-\hat{T}_2} (\hat{H} - i\hat{X}) e^{\hat{T}_2} | \Phi_{ij}^{ab} \rangle, \quad (11)$$

where $\hat{X} = X_\nu^\mu \hat{c}_\mu^\dagger \hat{c}_\nu$ with $X_\nu^\mu = \langle \psi_\mu | \dot{\psi}_\nu \rangle$, and those for orbitals as,

$$i|\dot{\psi}_p\rangle = (1 - \hat{P}) \hat{F}_p |\psi_p\rangle + |\psi_q\rangle X_p^q, \quad (12)$$

$$i \left\{ (\delta_b^a \rho_i^j - \rho_b^a \delta_i^j) X_j^b \right\} = F_j^a \rho_i^j - \rho_b^a F_b^{i*}, \quad (13)$$

where $\hat{P} = \sum_p |\psi_p\rangle \langle \psi_p|$, $F_q^p = \langle \phi_p | \hat{F}_q | \phi_q \rangle$, with

$$\hat{F}_p |\psi_p\rangle = \hat{h} |\psi_p\rangle + \hat{W}_s^r |\psi_q\rangle \rho_{or}^{qs} (\rho^{-1})_p^o, \quad (14)$$

$$W_s^r(\mathbf{x}_1) = \int d\mathbf{x}_2 \frac{\psi_r^*(\mathbf{x}_2) \psi_s(\mathbf{x}_2)}{|\mathbf{r}_1 - \mathbf{r}_2|}, \quad (15)$$

where ρ_q^p and ρ_{qs}^{pr} are the one- and two-body reduced density matrices, respectively, defined as

$$\rho_q^p = \langle \Phi | (1 + \hat{\Lambda}_2) e^{-\hat{T}_2} \hat{E}_q^p e^{\hat{T}_2} | \Phi \rangle, \quad (16)$$

$$\rho_{pr}^{qs} = \langle \Phi | (1 + \hat{\Lambda}_2) e^{-\hat{T}_2} \hat{E}_{qs}^{pr} e^{\hat{T}_2} | \Phi \rangle. \quad (17)$$

B. Derivation of TD-OMP2 as an approximation to TD-OCCD

Now we derive the TD-OMP2 method as an approximation to the TD-OCCD method, based on the partitioning of the electronic Hamiltonian,

$$\hat{H} = \hat{H}^{(0)} + \hat{H}^{(1)}, \quad (18a)$$

into the zeroth-order part $\hat{H}^{(0)} = \hat{f} = f_q^p \hat{E}_q^p$ and the perturbation $\hat{H}^{(1)} = \hat{H} - \hat{H}^{(0)}$, with

$$f_q^p = h_q^p + v_{qj}^{pj} = (h_0)_q^p + v_{qj}^{pj} + (V_{\text{ext}})_q^p, \quad (18b)$$

where $(h_0)_\nu^\mu$ and $(V_{\text{ext}})_\nu^\mu$ are the matrix elements of \hat{h}_0 and \hat{V}_{ext} , respectively.

Based on this partitioning, we apply the Baker-Campbell-Hausdorff expansion to TD-OCCD Lagrangian of Eq. (8), and retain those terms up to quadratic in v , τ , and λ (thus, contributing to first- and second-order corrections to Lagrangian) to obtain

$$L = L_0 - i\lambda_{ab}^{ij} \dot{\tau}_{ij}^{ab} + \langle \Phi | \hat{\Lambda}_2 (\hat{H} - i\hat{X}) | \Phi \rangle + \langle \Phi | [\hat{H} - i\hat{X}, \hat{T}_2] | \Phi \rangle + \langle \Phi | \hat{\Lambda}_2 [\hat{f} - i\hat{X}, \hat{T}_2] | \Phi \rangle, \quad (19)$$

where $L_0 = \langle \Phi | (\hat{H} - i\hat{X}) | \Phi \rangle$ is the reference contribution. Inserting this TD-OMP2 Lagrangian into Eq. (9) and making it stationary with respect to amplitude variations derives TD-OMP2 amplitude equations,

$$i\dot{\tau}_{ij}^{ab} = v_{ij}^{ab} - p(ij) \bar{f}_j^k \tau_{ik}^{ab} + p(ab) \bar{f}_c^a \tau_{ij}^{cb}, \quad (20)$$

$$-i\dot{\lambda}_{ab}^{ij} = v_{ab}^{ij} - p(ij) \bar{f}_i^k \lambda_{ab}^{kj} + p(ab) \bar{f}_a^c \lambda_{cb}^{ij}, \quad (21)$$

$$\dot{f}_q^p = f_q^p - iX_q^p, \quad (22)$$

where $p(\mu\nu)$ is the cyclic permutation operator. Importantly, Eqs. (20) and (21) reveals that the EOM for λ_{ab}^{ij} is just complex conjugate of that for τ_{ij}^{ab} , resulting in $\lambda_{ab}^{ij} = \tau_{ij}^{ab*}$. Therefore, we do not need a separate solution for the Λ_2 amplitudes.

We also make the action stationary with respect to the orthonormality-conserving orbital variation to derive formally the same orbital EOMs as Eqs. (12) and (13), with one-particle reduced density matrices (1RDM) and two-particle reduced density matrices (2RDM) given explicitly as

$$\rho_p^q = (\rho_0)_p^q + \gamma_p^q, \quad (23)$$

$$\rho_{pr}^{qs} = (\rho_0)_{pr}^{qs} + \Gamma_{pr}^{qs}, \quad (24)$$

where $(\rho_0)_p^q = \delta_j^q \delta_p^j$ and $(\rho_0)_{pr}^{qs} = \gamma_p^q \delta_j^s \delta_r^j + \gamma_r^s \delta_j^q \delta_p^j - \gamma_r^q \delta_j^s \delta_p^j - \gamma_p^s \delta_j^q \delta_r^j + \delta_j^q \delta_p^j \delta_k^s \delta_r^k - \delta_j^s \delta_p^j \delta_k^q \delta_r^k$ are the reference

contributions, and non-zero elements of γ_p^q and Γ_{pr}^{qs} are given by

$$\gamma_j^i = -\frac{1}{2} \lambda_{cb}^{ki} \tau_{kj}^{cb}, \quad \gamma_a^b = \frac{1}{2} \lambda_{ca}^{kl} \tau_{kl}^{cb}, \quad (25)$$

$$\Gamma_{ij}^{ab} = \tau_{ij}^{ab}, \quad \Gamma_{ab}^{ij} = \lambda_{ab}^{ij}. \quad (26)$$

In summary, the TD-OMP2 method is defined by the EOMs of double excitation amplitudes τ_{ij}^{ab} [Eq. (20)], the relation $\lambda_{ab}^{ij} = \tau_{ij}^{ab*}$, and the EOMs of orbitals [Eqs. (12) and (13)] with 1RDM and 2RDM elements given by Eqs. (23)-(26). The orbital time-derivative terms $-iX$ can be dropped from Eq. (22), if one makes an arbitrary choice of $\langle \psi_i | \dot{\psi}_j \rangle = \langle \psi_a | \dot{\psi}_b \rangle = 0$ for the redundant orbital rotations. It should be noted that (i) our partitioning scheme [Eqs. (18)] is consistent with the standard Møller-Plesset perturbation theory in the absence of the external field V_{ext} , and (ii) in case with V_{ext} , the zeroth-order Hamiltonian is time dependent, both through the change of orbitals and an explicit time dependence of $V_{\text{ext}}(t)$, the latter implying nonperturbative inclusion of the laser-electron interaction.

C. Alternative derivation

Another, more perturbation theoretic derivation begins with the following Lagrangian,

$$L = L_0 - i\lambda_{ab}^{ij} \dot{\tau}_{ij}^{ab} + \langle \Phi | \{ (1 + \hat{T}_2^\dagger) (\hat{f}_N - i\hat{X}) (1 + \hat{T}_2) + \hat{T}_2^\dagger \hat{v}_N + \hat{v}_N \hat{T}_2 \} | \Phi \rangle_c, \quad (27)$$

where the subscript c implies restriction to connected terms, and \hat{f}_N and \hat{v}_N are the normal-ordered part of \hat{f} and \hat{v} , respectively. Then we follow the procedure of time-dependent variational principle based on the action of Eq. (9), to obtain identical method as derived in the previous section. Two expressions of the TD-OMP2 Lagrangian, Eqs. (19) and (27), take the same numerical value as a function of time when evaluated with the solution of TD-OMP2, $\{\tau_{ij}^{ab}(t), \psi_p(t)\}$. The Lagrangian of Eq. (27) can be viewed as the time-dependent extension of the Hylleraas energy functional used in conventional, time-independent OMP2 method.^{58,59}

III. NUMERICAL RESULTS AND DISCUSSION

A. Ground-state energy of BH

To assess the performance of the method described in the previous section, we do a series of the ground-state energy calculations taking BH molecule as an example with double- ζ plus polarization (DZP) basis.⁶³ The imaginary time relaxation method⁴³ is used to obtain the ground state. We have started our calculations with the bond length of 1.8 a.u. and gradually increased to

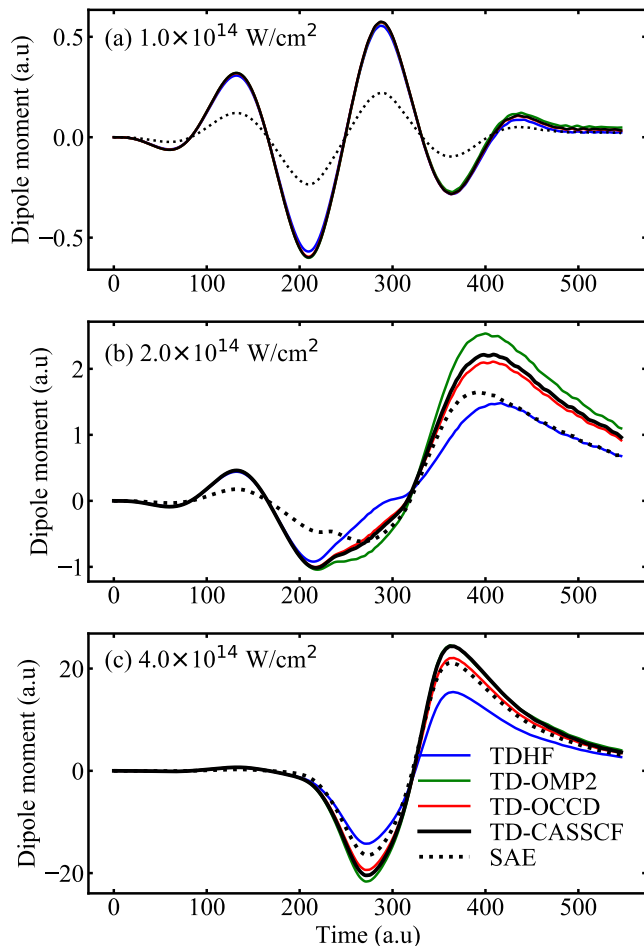


FIG. 1. Time evolution of sign-flipped dipole moment $\langle z \rangle$ of Ar irradiated by a laser pulse with a wavelength of 1200 nm and a peak intensity of 1×10^{14} W/cm² (a), 2×10^{14} W/cm² (b) and 4×10^{14} W/cm² (c), calculated with TDHF, TD-OMP2, TD-OCCD, TD-CASSCF, and SAE methods.

7.0 a.u., beyond which we could not achieve convergence. The values for both the MP2 and OMP2 are reported in Table I. The required matrix elements are obtained from the Gaussian09 program⁶² package and interfaced with our numerical code. All the values are compared with the values from the PSI4 program package.⁶¹ We obtained identical results for the reported values except in five cases, even for which the difference appears only at the eighth or ninth digit after the decimal point. In these calculations, the number of orbitals N are taken to be the same as the number of basis n_{bas} to make a comparison with PSI4,⁶¹ and all the orbitals are treated as active. However, our implementation allows to optimize orbitals with $N \leq n_{\text{bas}}$ in general, with a flexible classification of the occupied orbital space into frozen core, dynamical core, and active.

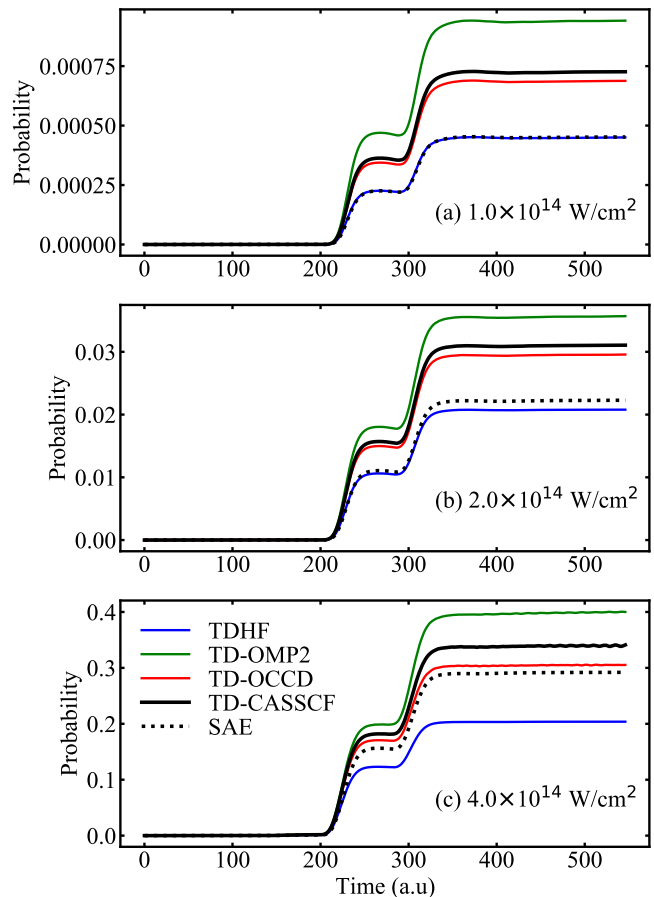


FIG. 2. Time evolution of single ionization probability of Ar irradiated by a laser pulse with a wavelength of 1200 nm and a peak intensity of 1×10^{14} W/cm² (a), 2×10^{14} W/cm² (b) and 4×10^{14} W/cm² (c) calculated with TDHF, TD-OMP2, TD-OCCD, TD-CASSCF, and SAE methods.

B. Ar in a strong laser field

We present numerical applications of the present method to Ar subject to an intense laser pulse linearly polarized in the z direction. Calculations for intense long-wavelength laser fields are computationally demanding, thus serving as a good test for the newly implemented methods. The laser-electron interaction is introduced to the one-body part of the electronic Hamiltonian within the dipole approximation in the velocity gauge,

$$h(\mathbf{r}, \mathbf{p}) = \frac{1}{2} |\mathbf{p}|^2 - \frac{Z}{|\mathbf{r}|} + A(t)p_z, \quad (28)$$

where $Z (= 18)$ is the atomic number, $A(t) = -\int^t E(t') dt'$ is the vector potential, with $E(t)$ being the laser electric field. While our method is gauge-invariant, we obtain faster convergence with the velocity gauge for the case of intense long-wavelength laser pulses^{34,40}.

The laser electric field is of the following form

$$E(t) = E_0 \sin(\omega_0 t) \sin^2\left(\pi \frac{t}{3T}\right), \quad (29)$$

for $0 \leq t \leq 3T$, and $E(t) = 0$ otherwise, with the central wavelength $\lambda = 2\pi/\omega_0 = 1200$ nm, the period $T = 2\pi/\omega_0 \sim 4.00$ fs, and the peak intensity $I_0 = E_0^2$. We have considered three different intensities of 1, 2, and 4×10^{14} W/cm² for Ar.

The spherical finite-element discrete variable representation (FEDVR) basis^{34,40} is used in our implementation. The convergence with respect to the maximum angular momentum l_{\max} is checked at the TDHF level, and l_{\max} is set to 72. The radial coordinate r is discretized by FEDVR consisting of 78 finite elements with 23 DVR functions each, to support $0 < r < R_{\max} = 300$. A $\cos^{\frac{1}{4}}$ mask function is switched on at 240 to avoid reflection from the boundary. Fourth-order exponential Runge-Kutta integrator⁶⁴ is used to propagate equations of motions with 20000 time steps per optical cycle. The simulations are continued after the end of pulse for further 6000 time steps.

For *ab initio* TDHF, TD-OMP2, TD-OCCD, and TD-CASSCF methods, the $1s2s2p$ core is kept frozen, and the dynamics of remaining eight electrons are actively taken into account with four (TDHF) or thirteen (TD-OMP2, TD-OCCD, and TD-CASSCF) active orbitals. The SAE method first diagonalizes the following effective Hamiltonian^{65,66}

$$h_{\text{eff}} = \frac{1}{2}|\mathbf{p}|^2 + V_{\text{eff}}(|\mathbf{r}|), \quad (30)$$

on the FEDVR basis, where the effective potential $V_{\text{eff}}(r)$ is taken to be^{65,66}

$$V_{\text{eff}}(r) = -\frac{1}{r} \{1 + Ae^{-r} + (Z-1-A)e^{-Br}\}, \quad (31)$$

with $A = 5.4$ and $B = 3.682$ for Ar⁶⁶. This potential correctly supports $1s$, $2s$, $2p$, $3s$, and $3p$ bound orbitals, with the $3p$ orbital energy of -15.82 eV with the present FEDVR basis. After obtaining the ground state, we solve the effective one-electron Schrödinger equation,

$$i\frac{d}{dt}|\chi\rangle = \hat{Q}\{h_{\text{eff}} + A(t)p_z\}|\chi\rangle, \quad (32)$$

starting from the $3p_0$ orbital. The projector $\hat{Q} = 1 - \sum_j |\phi_j\rangle\langle\phi_j|$, with ϕ_j running over $1s$, $2s$, $2p$, $3s$, and $3p_{\pm}$ orbitals [multiplied by the gauge factor $e^{-iA(t)z}$], keeps $\chi(t)$ orthonormal to the inner shell orbitals.

In Fig. 1, we plot the time evolution of the sign-flipped dipole moment $\langle z \rangle$ evaluated as a trace $\langle z \rangle = \langle \psi_p | \hat{z} | \psi_q \rangle \rho_p^q$ for *ab initio* methods and $\langle z \rangle = \langle \chi | z | \chi \rangle$ for SAE. We compare the TD-OMP2 results with SAE, TDHF, TD-OCCD, and TD-CASSCF ones. Within the same active space, TD-CASSCF produces highly accurate results, useful for performance analysis of the TD-OMP2 method.

The lowest (1.0×10^{14} W/cm²) and highest (4.0×10^{14} W/cm²) intensity cases characterize the dynamics with small and substantial amount of ionization, respectively (Fig. 2 below). The SAE approximation is known^{26,27,65} to work better for the latter case, where the dynamics is dominated by tunneling ionization of the single, most weakly bound electron (one of the $3p_0$ electrons in the present case). It is not well suited for describing the former case dominated by collective bound dynamics. On the other hand, TDHF serves as the reference multielectron method without the (Coulomb) correlation by definition, and provides a qualitatively correct description of the bound dynamics. It, however, fails to accurately describe cases with sizable tunneling ionization. (See, e.g., Ref. 67 and references therein.) These trends of SAE and TDHF methods are well confirmed in the performance comparison to the reference TD-CASSCF method in Figs. 1 and 2.

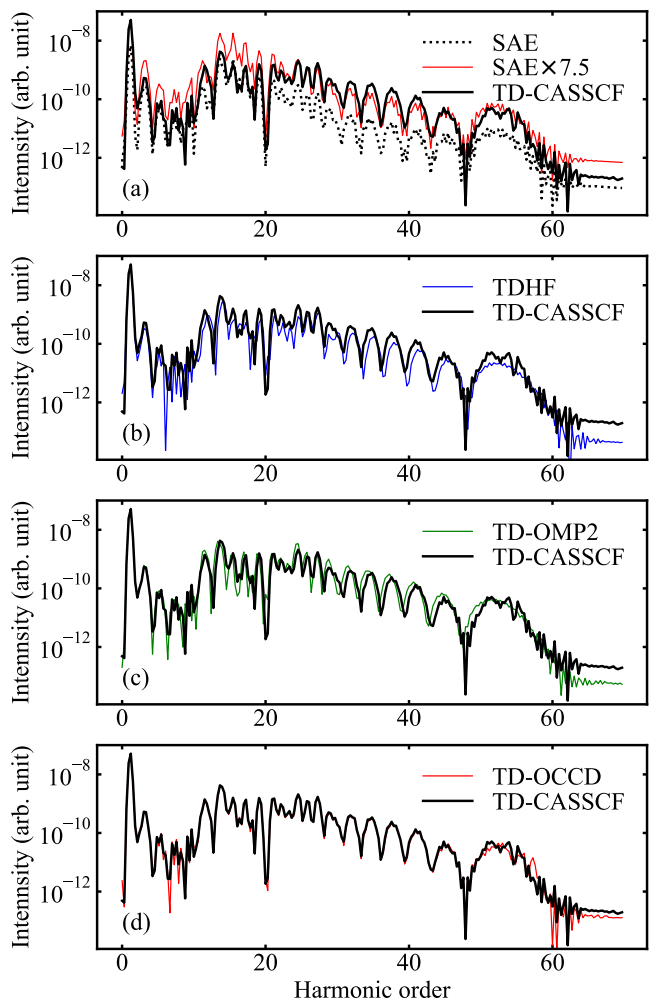


FIG. 3. The HHG spectra from Ar irradiated by a laser pulse with a wavelength of 1200 nm and a peak intensity of 1×10^{14} W/cm². Comparison of the results of SAE (a), TDHF (b), TD-OMP2 (c), and TD-OCCD (d) methods with that of TD-CASSCF.

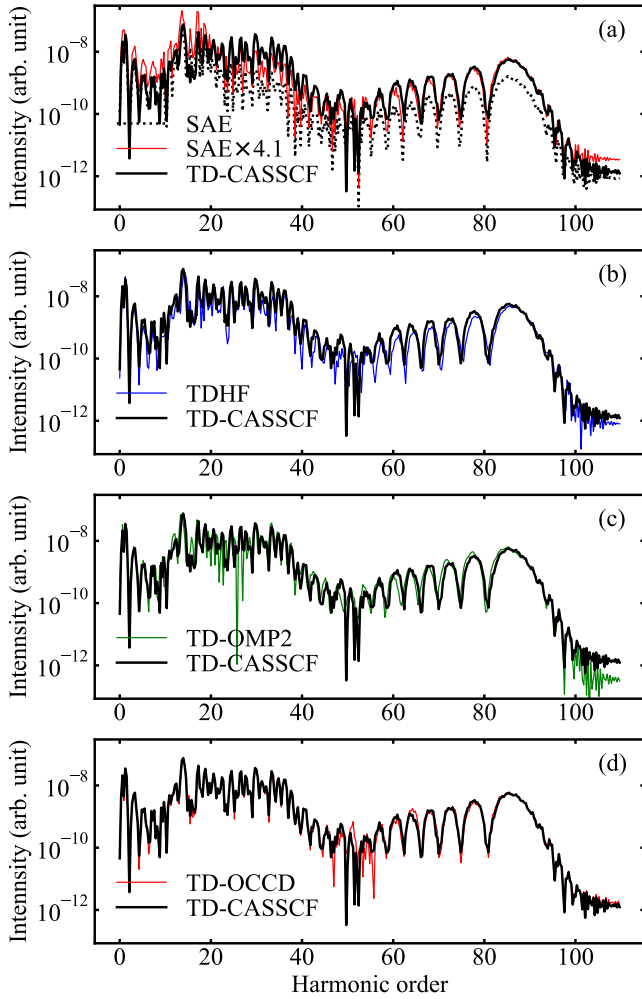


FIG. 4. The HHG spectra from Ar irradiated by a laser pulse with a wavelength of 1200 nm and a peak intensity of 2×10^{14} W/cm². Comparison of the results of SAE (a), TDHF (b), TD-OMP2 (c), and TD-OCCD (d) methods with that of TD-CASSCF.

As seen in Fig. 1-(a), at the lowest intensity of 10^{14} W/cm² all the methods except for SAE produce similar results. The TD-OCCD produces virtually the identical result with the TD-CASSCF, whereas TD-OMP2 slightly overestimates, and TDHF underestimates, considering TD-CASSCF as the benchmark. With increase in intensity, the difference among the methods become more prominent. While all the methods except for SAE give similar results in the early stage, TD-OMP2 and TDHF start to overestimate and underestimate, respectively, with the progress of tunneling ionization (Fig. 2). In general, the performance of the TD-OMP2 method is better than TDHF and SAE due to consideration at least a part of the electron correlation. It is noticed that the TD-OMP2 dipole moment agrees better with the TD-CASSCF one for the highest intensity [Fig. 1-(c)] than for the intermediate one [Fig. 1-(b)], which might indicate that the latter case, with both sizable ionization and

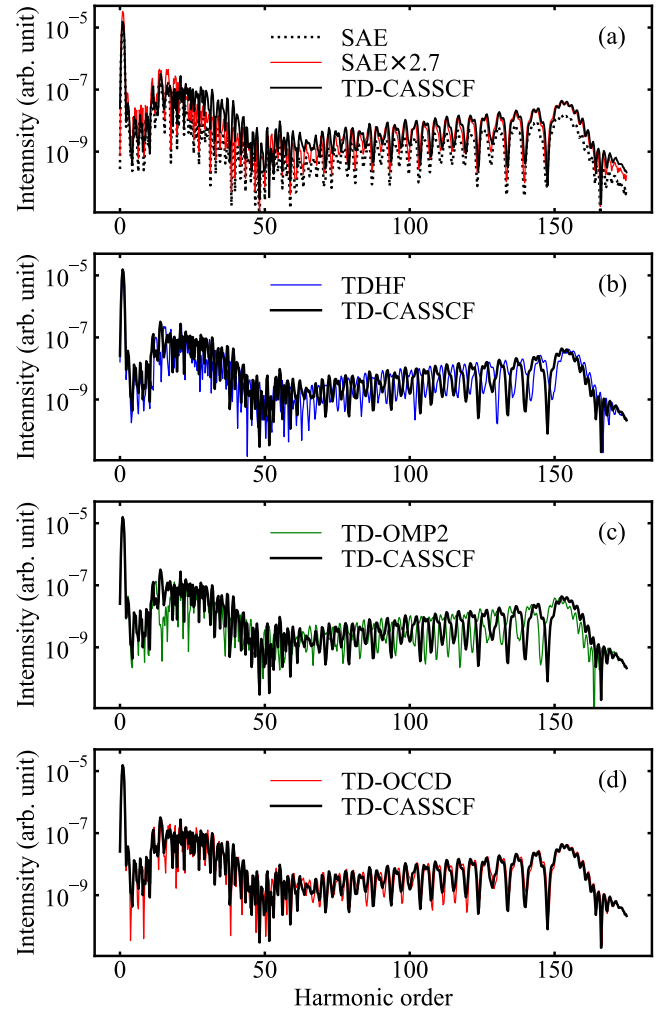


FIG. 5. The HHG spectra from Ar irradiated by a laser pulse with a wavelength of 1200 nm and a peak intensity of 4×10^{14} W/cm². Comparison of the results of SAE (a), TDHF (b), TD-OMP2 (c), and TD-OCCD (d) methods with that of TD-CASSCF.

nontrivial correlation effects coexisting, is theoretically more challenging.

The general trends in Fig. 1 are also found in the single ionization probability (Fig. 2), evaluated as the probability of finding an electron outside a sphere of 20 a.u. radius. Again, we see a systematic overestimation by TD-OMP2 and underestimation by TDHF in comparison to the TD-CASSCF result; the performance of TD-OMP2 is better than that of TDHF and SAE, except for the highest intensity case, where the SAE result is as accurate as the TD-OCCD one.

In Figs. 3-5 we compare HHG spectra, calculated as the modulus squared of the Fourier transform of the expectation value of the dipole acceleration, which, in turn, is obtained with a modified Ehrenfest expression³⁴. All *ab initio* methods reproduce the HHG spectra relatively well, including an experimentally observed char-

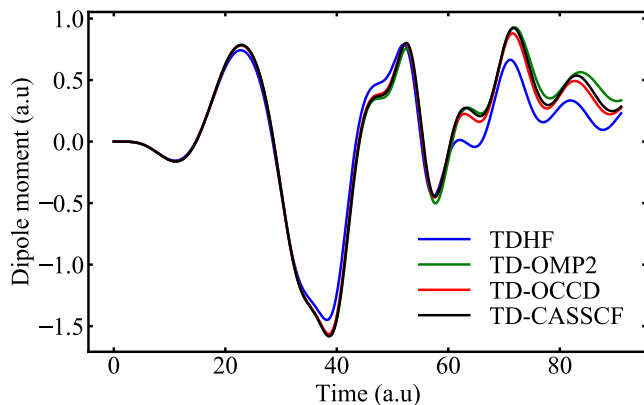


FIG. 6. Time evolution of sign-flipped dipole moment $\langle z \rangle$ of Ar irradiated by a laser pulse with a wavelength of 200 nm and a peak intensity of 4×10^{14} W/cm², calculated with TDHF, TD-OMP2, TD-OCCD, and TD-CASSCF methods.

acteristic dip around the 52nd order (~ 54 eV) at $2 \times$ and 4×10^{14} W/cm² related to the Cooper minimum of the photoionization spectrum⁶⁸ at the same energy. However, TDHF systematically underestimates and fails to reproduce fine details. The SAE method severely underestimates the HHG yields, although the overall shape of the HHG spectrum is well reproduced, and an intensity-dependent scaling brings the spectral intensity at the higher plateau close to that of TD-CASSCF, especially for the highest intensity. The agreement with the TD-CASSCF results is much better for the TD-OCCD method, which contains nonlinear terms in the amplitude equations, then followed by TD-OMP2 with slight overestimation. This trend is consistent with the capability of each method to treat the electron correlation.

In order to investigate the performance of TD-OMP2 method for shorter wavelengths, where electrons not only in the highest-occupied but also in the inner-shell orbitals are driven by the laser, we consider a shorter wavelength of 200 nm with an intensity of 4×10^{14} W/cm². All the other simulation parameters are identical to those given above. The obtained time evolution of the dipole moment (Fig. 6) shows a slight overestimation of the oscillation

TABLE II. Comparison of the CPU time^a (in second) spent for the evaluation of the T_2 equation, Λ_2 equation, and 2RDM for TD-OCCD and TD-OMP2 methods

TD-OCCD			TD-OMP2		
T_2	Λ_2	2RDM	T_2	Λ_2	2RDM
40.8	55.5	109.5	1.11	-	0.25

^a CPU time spent for the simulation of Ar atom for 1000 time steps ($0 \leq t \leq 0.05T$) of a real-time simulation ($I_0 = 4 \times 10^{14}$ W/cm² and $\lambda = 1200$ nm.), using an Intel(R) Xeon(R) CPU with 12 processors having a clock speed of 3.33GHz.

amplitude by TD-OMP2 and underestimation by TDHF compared to the TD-CASSCF result as in the case for the longer wavelength. It is encouraging, however, that the TD-OMP2 result is much closer to the TD-CASSCF one for the shorter wavelength, which is more sensitive to the treatment of correlation effects.

It is worth noting that, for an intensity as high as 4×10^{14} W/cm², the TD-OMP2 simulation completed stably. This should be the direct consequence of full inclusion of the laser-electron interaction in the zeroth-order Hamiltonian and the orbital optimization (propagation) according to the time-dependent variational principle based on the total (up to second-order) Lagrangian, which keeps the instantaneous *perturbation* $\hat{H}^{(1)} = \hat{H} - \hat{f}$ relatively small in the present simulation.

Finally, the computational cost of different parts of TD-OMP2 and TD-OCCD methods are compared in Table II for the same computational condition as in Fig. 3 (c). The evaluation of T_2 equation, Λ_2 equation, and 2RDM all scale as N^6 for the TD-OCCD method. On the other hand, for the TD-OMP2 method, the evaluation of T_2 equation scales as N^5 , and we do not need a separate solution for Λ_2 , as it is just the complex conjugate of T_2 . The greatest time saving for the TD-OMP2 method comes from the evaluation of 2RDM since it scales as N^4 , and does not involve any operator products. Overall, TD-OMP2 achieves a significant cost reduction compared to TD-OCCD, making it an attractive choice for simulations involving larger chemical systems.

IV. CONCLUSION

We have successfully implemented the TD-OMP2 method for the real-time simulations of laser-induced dynamics in relatively large chemical systems. The TD-OMP2 method retains the size-extensivity and gauge-invariance of TD-OCC, and is computationally much more efficient than the full TD-OCCD method. As a first numerical test, we have applied the method to the ground state of BH and the laser-driven dynamics of Ar. The imaginary time relaxation for BH obtains the identical ground-state energies with those by the stationary theory, which indicates the correctness of the implementation. The performance of the present method is numerically investigated in comparison to SAE, TDHF, TD-OCCD, and TD-CASSCF methods for the case of laser-driven Ar. The results suggest a decent performance with a consistent overestimation of the correlation effect in such highly nonlinear phenomena. Remarkably, the TD-OMP2 method is stable and does not breakdown even in the presence of strong laser-electron interaction, thanks to the nonperturbative inclusion of external fields and time-dependent orbital optimization. Further assessment of the TD-OMP2 method for different systems and severer simulation conditions (e.g, with higher-intensity and/or longer-wavelength lasers) will be reported elsewhere.

ACKNOWLEDGMENTS

This research was supported in part by a Grant-in-Aid for Scientific Research (Grants No. 17K05070, No. 18H03891, and No. 19H00869) from the Ministry of Education, Culture, Sports, Science and Technology (MEXT) of Japan. This research was also partially supported by JST COI (Grant No. JPMJCE1313), JST CREST (Grant No. JPMJCR15N1), and by MEXT Quantum Leap Flagship Program (MEXT Q-LEAP) Grant Number JPMXS0118067246.

DATA AVAILABILITY

The data that support the findings of this study are available from the corresponding author upon reasonable request.

- ¹P. á. Corkum and F. Krausz, *Nature physics* **3**, 381 (2007).
- ²F. Krausz and M. Ivanov, *Reviews of Modern Physics* **81**, 163 (2009).
- ³J. Itatani *et al.*, *Nature* **432**, 867 (2004).
- ⁴E. Goulielmakis *et al.*, *Nature* **466**, 739 (2010).
- ⁵G. Sansone *et al.*, *Nature* **465**, 763 (2010).
- ⁶M. Schultze *et al.*, *Science* **328**, 1658 (2010).
- ⁷K. Klünder *et al.*, *Physical Review Letters* **106**, 143002 (2011).
- ⁸L. Belshaw *et al.*, *The journal of physical chemistry letters* **3**, 3751 (2012).
- ⁹F. Calegari *et al.*, *Science* **346**, 336 (2014).
- ¹⁰O. Smirnova *et al.*, *Nature* **460**, 972 (2009).
- ¹¹P. Antoine, A. L’huillier, and M. Lewenstein, *Physical Review Letters* **77**, 1234 (1996).
- ¹²K. L. Ishikawa and T. Sato, *IEEE Journal of Selected Topics in Quantum Electronics* **21**, 1 (2015).
- ¹³I. Tikhomirov, T. Sato, and K. L. Ishikawa, *Physical review letters* **118**, 203202 (2017).
- ¹⁴Y. Li, T. Sato, and K. L. Ishikawa, *Phys. Rev. A* **99**, 043401 (2019).
- ¹⁵S. Pabst and R. Santra, *Phys. Rev. Lett.* **111**, 233005 (2013).
- ¹⁶J. S. Parker, E. S. Smyth, and K. T. Taylor, *Journal of Physics B: Atomic, Molecular and Optical Physics* **31**, L571 (1998).
- ¹⁷J. S. Parker *et al.*, *Journal of Physics B: Atomic, Molecular and Optical Physics* **33**, L239 (2000).
- ¹⁸M. Pindzola and F. Robicheaux, *Physical Review A* **57**, 318 (1998).
- ¹⁹S. Laulan and H. Bachau, *Physical Review A* **68**, 013409 (2003).
- ²⁰K. L. Ishikawa and K. Midorikawa, *Physical Review A* **72**, 013407 (2005).
- ²¹J. Feist *et al.*, *Physical review letters* **103**, 063002 (2009).
- ²²K. L. Ishikawa and K. Ueda, *Physical review letters* **108**, 033003 (2012).
- ²³S. Sukiasyan, K. L. Ishikawa, and M. Ivanov, *Physical Review A* **86**, 033423 (2012).
- ²⁴W. Vanroose, D. A. Horner, F. Martin, T. N. Rescigno, and C. W. McCurdy, *Physical Review A* **74**, 052702 (2006).
- ²⁵D. A. Horner *et al.*, *Physical review letters* **101**, 183002 (2008).
- ²⁶J. Krause, *Phys. Rev. Lett.* **68**, 3535 (1992).
- ²⁷K. C. Kulander, *Physical Review A* **36**, 2726 (1987).
- ²⁸J. Caillat *et al.*, *Physical review A* **71**, 012712 (2005).
- ²⁹T. Kato and H. Kono, *Chemical physics letters* **392**, 533 (2004).
- ³⁰M. Nest, T. Klamroth, and P. Saalfrank, *The Journal of chemical physics* **122**, 124102 (2005).
- ³¹D. J. Haxton, K. V. Lawler, and C. W. McCurdy, *Physical Review A* **83**, 063416 (2011).
- ³²D. Hochstuhl and M. Bonitz, *The Journal of chemical physics* **134**, 084106 (2011).
- ³³T. Sato and K. L. Ishikawa, *Physical Review A* **88**, 023402 (2013).
- ³⁴T. Sato *et al.*, *Physical Review A* **94**, 023405 (2016).
- ³⁵H. Miyagi and L. B. Madsen, *Physical Review A* **87**, 062511 (2013).
- ³⁶H. Miyagi and L. B. Madsen, *Physical Review A* **89**, 063416 (2014).
- ³⁷D. J. Haxton and C. W. McCurdy, *Physical Review A* **91**, 012509 (2015).
- ³⁸T. Sato and K. L. Ishikawa, *Physical Review A* **91**, 023417 (2015).
- ³⁹J. J. Omiste, W. Li, and L. B. Madsen, *Phys. Rev. A* **95**, 053422 (2017).
- ⁴⁰Y. Orimo, T. Sato, A. Scrinzi, and K. L. Ishikawa, *Physical Review A* **97**, 023423 (2018).
- ⁴¹R. Anzaki, T. Sato, and K. L. Ishikawa, *Phys. Chem. Chem. Phys.* **19**, 22008 (2017).
- ⁴²A. U. J. Lode, C. Lévéque, L. B. Madsen, A. I. Streltsov, and O. E. Alon, *Rev. Mod. Phys.* **92**, 011001 (2020).
- ⁴³T. Sato, H. Pathak, Y. Orimo, and K. L. Ishikawa, *The Journal of chemical physics* **148**, 051101 (2018).
- ⁴⁴C. D. Sherrill, A. I. Krylov, E. F. Byrd, and M. Head-Gordon, *The Journal of chemical physics* **109**, 4171 (1998).
- ⁴⁵A. I. Krylov, C. D. Sherrill, E. F. Byrd, and M. Head-Gordon, *The Journal of chemical physics* **109**, 10669 (1998).
- ⁴⁶S. Kvaal, *The Journal of chemical physics* **136**, 194109 (2012).
- ⁴⁷J. Arponen, *Annals of Physics* **151**, 311 (1983).
- ⁴⁸H. Pathak, T. Sato, and K. L. Ishikawa, arXiv:2001.02206 .
- ⁴⁹W. Meyer, *International Journal of Quantum Chemistry* **5**, 341 (1971).
- ⁵⁰R. Ahlrichs, P. Scharf, and C. Ehrhardt, *The Journal of Chemical Physics* **82**, 890 (1985).
- ⁵¹F. Wennmohs and F. Neese, *Chemical Physics* **343**, 217 (2008).
- ⁵²F. Neese, F. Wennmohs, and A. Hansen, *The Journal of chemical physics* **130**, 114108 (2009).
- ⁵³C. Kollmar and F. Neese, *Molecular Physics* **108**, 2449 (2010).
- ⁵⁴J.-P. Malrieu, H. Zhang, and J. Ma, *Chemical Physics Letters* **493**, 179 (2010).
- ⁵⁵J. Čížek, *The Journal of Chemical Physics* **45**, 4256 (1966).
- ⁵⁶R. J. Bartlett, *Annual Review of Physical Chemistry* **32**, 359 (1981).
- ⁵⁷U. Bozkaya, J. M. Turney, Y. Yamaguchi, H. F. Schaefer III, and C. D. Sherrill, *The Journal of chemical physics* **135**, 104103 (2011).
- ⁵⁸L. Adamowicz and R. J. Bartlett, *The Journal of chemical physics* **86**, 6314 (1987).
- ⁵⁹F. Neese, T. Schwabe, S. Kossmann, B. Schirmer, and S. Grimme, *Journal of chemical theory and computation* **5**, 3060 (2009).
- ⁶⁰U. Bozkaya, *The Journal of chemical physics* **135**, 224103 (2011).
- ⁶¹J. M. Turney *et al.*, *Wiley Interdisciplinary Reviews: Computational Molecular Science* **2**, 556 (2012).
- ⁶²M. Frisch *et al.*, *Gaussian 09*, revision d. 01, 2009.
- ⁶³R. Harrison and N. Handy, *Chemical Physics Letters* **95**, 386 (1983).
- ⁶⁴M. Hochbruck and A. Ostermann, *Acta Numerica* **19**, 209 (2010).
- ⁶⁵H. G. Muller and F. C. Kooiman, *Phys. Rev. Lett* **81**, 1207 (1998).
- ⁶⁶K. Schiessl, E. Persson, A. Scrinzi, and J. Burgdörfer, *Physical Review A* **74**, 053412 (2006).
- ⁶⁷T. Sato and K. L. Ishikawa, *J. Phys. B: At. Mol. Opt. Phys.* **47**, 204031 (2014).
- ⁶⁸H. J. Wörner, H. Niikura, J. B. Bertrand, P. B. Corkum, and D. M. Villeneuve, *Phys. Rev. Lett.* **102**, 103901 (2009).